HHS Public Access

Author manuscript

Nat Med. Author manuscript; available in PMC 2011 July 01.

Published in final edited form as:

Nat Med. 2011 January ; 17(1): 130–134. doi:10.1038/nm.2268.

Differentiation between glioma and radiation necrosis using molecular magnetic resonance imaging of endogenous proteins and peptides

Jinyuan Zhou[1,2,*], **Erik Tryggestad**[3], **Zhibo Wen**[1,4], **Bachchu Lal**[5,6], **Tingting Zhou**[1], **Rachel Grossman**[7], **Silun Wang**[1], **Kun Yan**[1], **De-Xue Fu**[8], **Eric Ford**[3], **Betty Tyler**[7], **Jaishri Blakeley**[5], **John Laterra**[5,6], and **Peter C.M. van Zijl**[1,2]

[1]Department of Radiology, Johns Hopkins University School of Medicine, Baltimore, Maryland, USA.

[2]F.M. Kirby Research Center for Functional Brain Imaging, Kennedy Krieger Institute, Baltimore, Maryland, USA.

[3]Department of Radiation Oncology, Johns Hopkins University School of Medicine, Baltimore, Maryland, USA.

[4]Department of Radiology, Zhujiang Hospital, Southern Medical University, Guangzhou, Guangdong, China.

[5]Department of Neurology, Johns Hopkins University School of Medicine, Baltimore, Maryland, USA.

[6]Department of Neurology, Kennedy Krieger Institute, Baltimore, Maryland, USA.

[7]Department of Neurosurgery, Johns Hopkins University School of Medicine, Baltimore, Maryland, USA.

[8]Department of Oncology, Johns Hopkins University School of Medicine, Baltimore, Maryland, USA.

[*]Corresponding author: Jinyuan Zhou, Ph.D. Division of MR Research, Department of Radiology Johns Hopkins University School of Medicine 600 N. Wolfe Street, 336 Park Building Baltimore, MD 21287, U.S.A. Phone: (410) 955-7491 Fax: (410) 614-1977 jzhou@mri.jhu.edu.

AUTHOR CONTRIBUTIONS

J.Z. developed the APT methodology, designed and performed most of the MRI experiments, carried out data analysis, prepared figures, wrote the manuscript, and supervised the project. E.T. & E.F. designed and performed the radiation experiments and contributed to manuscript preparation. Z.W. contributed to MRI experimental work and histological analysis, contributed to manuscript preparation, and provided helpful discussions on related clinical issues. B.L. performed experimental work in the tumor models and performed pathology experiments. T.Z. contributed to MRI experimental work, statistical analysis, and manuscript preparation. R.G. & B.T. contributed to experimental work, especially in the tumor models, and manuscript preparation. S.W. contributed to MRI experimental work, performed histological analysis and statistical analysis, prepared some figures, and contributed to manuscript preparation. K.Y. & D.F. contributed to experimental work and data analysis. J.B. & J.L. contributed to experimental design and manuscript preparation and provided helpful discussions on related clinical issues. P.C.M.Z. developed the APT methodology, contributed to experimental design, and edited the manuscript.

COMPETING INTERESTS STATEMENT

The authors declare competing financial interests: details accompany the full-text HTML version of the paper at http://www.nature.com/naturemedicine/.

Abstract

Distinguishing tumor recurrence from radiation necrosis following brain tumor therapy remains a major clinical challenge. Here we demonstrate the ability to distinguish these lesions using the amide proton transfer (APT) MRI signals of endogenous cellular proteins and peptides as an imaging biomarker. When comparing two orthotopic glioma models (SF188/V+ glioma and 9L gliosarcoma) with a radiation necrosis model in rats, viable glioma (hyperintense) and radiation necrosis (hypointense to isointense) could be clearly differentiated using APT MRI. When irradiating rats with U87MG gliomas, the APT signals in the irradiated tumors decreased significantly at 3 days and 6 days post-radiation. The amide protons detected by APT provide a unique and non-invasive MRI biomarker for assessing viable malignancy versus radiation necrosis and predicting tumor response to therapy.

Keywords

Radiation necrosis; glioma; tumor recurrence; biomarker; APT imaging; molecular imaging; MRI

Advances in surgery, radiation therapy and chemotherapy have improved survival in patients with malignant gliomas. However, the most aggressive malignant gliomas remain universally fatal, with a median survival of approximately 15 months for glioblastoma multiforme and 2–5 years for anaplastic astrocytoma[1]. Magnetic resonance (MR) imaging (MRI) is a standard modality for neuroimaging. Of the most common MRI approaches used to evaluate brain tumors in the clinical setting, T_2-weighted or fluid-attenuated inversion recovery (FLAIR) images generally show increased water content, and gadolinium (Gd)-enhanced T_1-weighted images indicate blood-brain barrier disruption. In combination, they are used to determine the extent of involvement and to assess a therapeutic response[2]. Although Gd-enhanced MRI is a sensitive marker of blood-brain barrier disruption, it does not distinguish between the many etiologies that can cause such disruption, such as tumor regrowth and radiation necrosis (Supplementary Fig. 1)[3-5]. Similarly, T_2-weighted and FLAIR hyperintensities may be indicative of many abnormalities, including infiltrating tumor, vasogenic edema and radiation necrosis. Hence, standard MRI sequences provide excellent anatomic detail, but are non-specific.

The ability to reliably distinguish between tumor recurrence and radiation necrosis would have immediate clinical implications. Treatment-induced injury is treated conservatively, whereas tumor recurrence requires new anti-cancer therapies. Currently, the only reliable approach to differentiate these etiologies is tissue sampling via surgery. This is invasive and not always feasible. Even when surgery is possible and advised, choosing the area to target for tissue sampling can be very difficult, and pathology results may be variable, as gliomas are heterogeneous. Various advanced MR techniques[6-9] and nuclear medicine approaches[10,11] are being investigated in an effort to identify a more accurate imaging marker for tumor. However, the results have been mixed, and there is currently still no standard imaging modality available for differentiating tumor from radiation injury in the clinic[2]. Therefore, the development of imaging modalities that better identify targets for biopsy to improve diagnostic yield and reliably identify progressive tumor from various stages of treatment injury non-invasively remains an urgent need in neuro-oncology[12-15].

Recently, a new contrast mechanism for MRI, called chemical exchange-dependent saturation transfer[16], has emerged in the field of cellular and molecular imaging[17-19]. Based on this, we have designed a specific chemical exchange-based saturation transfer MRI technique, dubbed amide proton transfer (APT) imaging[20], which can be used to detect the amide protons of endogenous, low-concentration mobile proteins and peptides in tissue[21], such as those in the cytoplasm. Malignant gliomas are highly cellular tumors and have a higher cellular content of proteins and peptides, as revealed by MRI-guided proteomics[22] and *in vivo* MR spectroscopy[23]. Here, we show that the amide protons detected by APT provide an imaging biomarker that can distinguish between tumor and radiation necrosis non-invasively in animal models, where controlled radiopathologic correlation can be readily performed. Because APT imaging does not require exogenous contrast agents, it can be incorporated into standard clinical MRI protocols using existing hardware[24]. The successful clinical translation of APT imaging would reduce the misdiagnosis of tumor recurrence versus radiation necrosis and improve patient care.

RESULTS

Radiation necrosis and glioma show similar features on conventional MR images

We first established a brain radiation necrosis model in rats and evaluated its MRI characteristics on conventional T_2-weighted and Gd-enhanced T_1-weighted images, which are routinely used in the clinic. The left hemispheres of adult rats (Fischer 344; $n = 10$) were irradiated with a single dose of 40 Gy in an area of 10×10 mm^2 using a small animal radiation research platform[25]. One rat was euthanized in the animal care facility at 101 days post-radiation due to severe eye infection. In all other rats, radiation-induced necrosis began to appear at ~5 months post-radiation, and APT data were acquired during days 163–189. These rats developed large necrotic lesions that were heterogeneous on the T_2-weighted images (Fig. 1a) and had high Gd enhancement on the post-contrast T_1-weighted images (Fig. 1b). Necrotic lesions included several injured white matter tracts (fornix, external capsule, internal capsule and cerebral peduncle) and gray matter (caudate putamen).

Two rat brain tumor models (SF188/V+ and 9L) were used to compare viable neoplasm with radiation necrosis (Fig. 2). The SF188/V+ xenografts are a human glioma model transfected with mouse full-length VEGF164 cDNA[26]. The SF188/V+ tumors grew in all rats ($n = 9$) with variable growth rates. MRI was performed 9–35 days post-implantation, when the tumors were 3–5 mm in diameter. The SF188/V+ xenografts were quite heterogeneous on the T_2-weighted images (Fig. 2b), similar to high-grade gliomas in patients. In addition, the tumor xenografts showed enhancement on the Gd-enhanced T_1-weighted images. For the 9L gliosarcoma group ($n = 9$), MRI was performed 10–12 days post-implantation, when the tumors were 3–5 mm in diameter. The 9L tumors were hyperintense on the T_2-weighted images with large Gd enhancement (Fig. 2c). Therefore, analogous to the clinical situation (Supplementary Fig. 1), radiation-induced necrosis and both brain tumor models had similar imaging features (T_2-abnormality, Gd enhancement and mass effect) that could generally not be used to distinguish between the different pathological processes.

Radiation necrosis and glioma can be differentiated by APT imaging

The APT effect is measured as a reduction in bulk water intensity due to chemical exchange of water protons with labeled backbone amide protons of endogenous mobile proteins and peptides in tissue[20,21]. Thus, specific molecular information is obtained indirectly through the bulk water signal usually used in imaging. Such labeling is accomplished using selective radiofrequency irradiation at the MR frequency of the backbone amide protons, ~3.5 ppm downfield of the water resonance, causing saturation (or signal destruction) that is transferred to water protons[20,21]. Typically, there are multiple saturation effects that are ongoing in tissue, including direct water saturation and conventional magnetization transfer from semi-solid tissue components, and the APT signal must be separated out. The sum of all saturation effects is generally called the magnetization transfer ratio, $MTR = 1 - S_{sat}/S_0$, where S_{sat} and S_0 are the signal intensities with and without selective irradiation. The APT signal is measured through referencing of the saturation effects at the amide proton frequency (+3.5 ppm with respect to the water proton MR frequency) with effects at −3.5 ppm from the water signal: MTR(+3.5ppm) - MTR(−3.5ppm). The resulting images are called the APT images.

We compared the appearance of APT, Gd-enhanced T_1-weighted images and histology in the radiation necrosis and tumor models (Fig. 3). We used Gd-enhanced T_1-weighted images to identify lesions. These Gd-enhanced images appeared similar for all three pathologies, showing hyperintense areas that could be used to identify but not distinguish lesions. Hematoxylin and eosin (H&E) staining of histological brain sections was performed to confirm the presence of the radiation necrosis and viable tumors. In all cases of radiation necrosis, APT MRI signals were hypointense to isointense in the injured areas (as identified by Gd-enhanced T_1-weighted images) with respect to the contralateral uninjured brain (Fig. 3a). There were “dark” necrotic cores with a hypointense APT signal (black arrow) in these injured areas. The necrotic cores corresponded to the centers of the Gd-enhancing regions on the T_1-weighted images. The Gd-enhancing regions extended outside the necrotic cores, where APT was isointense with respect to the contralateral brain tissue. Low-magnification histology images (1.25×) revealed radiation-induced morphological changes, such as parenchymal coagulative necrosis (the cardinal characteristic of radiation necrosis). This necrotic change was found in the ipsilateral hemisphere, specifically in the white matter of the fornix, external capsule, internal capsule and cerebral peduncle. High-magnification histology (20×) clearly showed the loss of normal brain tissue components with vacuolation changes of necrosis, particularly in the necrotic cores. Necrotic cells and damaged vessels were also seen in these regions.

In contrast, APT imaging of both the SF188/V+ (Fig. 3b) and 9L (Fig. 3c) tumors showed hyperintensities (pink arrow and red arrow, respectively) in the most viable, actively growing tumor areas, as identified by the Gd-enhanced T_1-weighted images. Coronal histological sections clearly showed tumor masses, consisting of high density and relatively homogeneously distributed malignant cells. The tumor contours in the low-magnification (1.25×) histology images matched those in the Gd-enhanced T_1-weighted and APT images. Furthermore, consistent with our previous APT studies on animals[21] and humans[24], the APT signals were consistently low in the peritumoral areas without Gd enhancement, such as in

the peritumoral edema and ventricles. Thus, APT hyperintensity is a unique feature of brain tumors. The above results demonstrate that, although radiation-induced necrosis and viable gliomas show similar T_2 hyperintense and Gd-enhanced MRI characteristics, these two pathologies have markedly different APT images, namely, hypointensity to isointensity for radiation necrosis (Fig. 3a) versus hyperintensity for tumors (Fig. 3b,c). This unique visual difference clearly indicates that the APT signal of endogenous cellular proteins and peptides can be used to distinguish active tumor from treatment-induced injury, such as radiation necrosis.

Quantitative analysis of APT MRI signal intensities

The APT images of two rat brain tumor models (SF188/V+ and 9L) were compared with radiation necrosis in a quantitative manner (Fig. 4). In the radiation-injured brain, the average APT intensity was −3.6% ± 0.4% in Gd-enhancing necrotic cores and −2.8% ± 0.3% in contralateral brain areas. The observed APT MRI contrast between the necrotic cores and the contralateral brain tissue, therefore, was small (−0.8%), but still significant (95% confidence interval, −1.3% to −0.4%; $P < 0.01$; $n = 9$). In the SF188/V+ model, the average tumor APT signal was 12.2% ± 4.6%, which was significantly higher than that observed in the contralateral brain (−1.5% ± 0.6%; $P < 0.001$; $n = 9$). The average APT MRI contrast between tumor and contralateral brain tissue was 13.7% (95% confidence interval, 10.3% to 17.2%). In the 9L model, the APT imaging intensity also was significantly higher in the tumor (2.7% ± 0.7%) than in the contralateral brain tissue (−1.7% ± 0.9%; $P < 0.001$; $n = 9$), leading to an average APT contrast of 4.4%, with a 95% confidence interval of 3.7% to 5.1%.

The comparison between the groups showed that the average APT intensities of the two tumors were all significantly higher than those of radiation-induced necrosis (all $P < 0.001$, Fig. 4). The APT contrast between SF188/V+ tumor and radiation necrosis was largest, namely, 15.8%, with a 95% confidence interval from 12.8% to 18.8%. For the 9L tumor, APT contrast with radiation necrosis was 6.3% (95% confidence interval, 5.8% to 6.8%). The APT signals provide a reliable non-invasive imaging biomarker for the assessment of viable malignancy versus radiation-induced brain injury, which are often indistinguishable with routine MRI approaches (Supplementary Table 1).

APT MRI can distinguish viable tumor from necrosis within an irradiated tumor

We further applied APT imaging to U87MG tumor-bearing rats ($n = 5$) treated with radiation therapy. Prior to radiation (within one day), baseline MRI was performed. On post-implantation day 11, when lesions were 4–7 mm in diameter, the tumors were irradiated with a single dose of 40 Gy to a 10 × 10 mm^2 region under image guidance with planar radiographs. Follow-up MRI was performed 3 days and 6 days post-radiation. At baseline, U87MG tumors were hyperintense with respect to contralateral brain tissue on APT images (Fig. 5a, Supplementary Fig. 2). Although the irradiated tumors appeared to enlarge during the first several days post-radiation, their APT signals gradually decreased following therapy, corresponding to a clear left shift of the APT histogram (Supplementary Fig. 3). On post-radiation day 6, the APT intensity of the irradiated tumors became quite heterogeneous (hyperintense to isointense). These irradiated tumors clearly showed the presence of large

necrotic areas upon histopathological analysis, in contrast to un-irradiated U87MG tumors that typically display no spontaneous necrosis[27].

Quantitatively, the average APT intensities of the U87MG tumors were 3.1% ± 0.3% pre-radiation, 2.1% ± 0.5% at 3 days post-radiation, and 0.6% ± 1.1% at 6 days post-radiation (Fig. 5b). This corresponds to a decrease in APT intensity of 1.1% (95% confidence interval, 0.6% to 1.6%; $P < 0.05$) at 3 days post-radiation and 2.5% (95% confidence interval, 1.5% to 3.5%; $P < 0.001$) at 6 days post-radiation. Importantly, several commonly used MRI parameters did not detect significant changes during this early period post-radiation (Supplementary Table 2). Particularly, contrary to expectation, there was a transient decrease in apparent diffusion coefficient (ADC) at 3 days post-radiation. However, the mean ADC values in tumor increased at later time points, in line with pre-clinical and clinical data (Supplementary Fig. 3, Supplementary Discussion)[28]-[30]. These results clearly show that the APT signals can potentially provide an early, sensitive imaging biomarker for the evaluation of tumor response to radiation therapy.

DISCUSSION

Many types of tumor cells proliferate rapidly and have a higher cellular content of proteins and peptides than normal cells. Recently, in an MRI-proteomics correlation experiment, Hobbs et al.[22] found that protein expression profiles correlated with Gd enhancement in human glioblastoma multiforme. More protein species and higher protein expression levels were seen in Gd-enhancing regions than in non-enhancing regions. Using single-voxel, *in vivo* proton MR spectroscopy, Howe et al.[23] showed that the MR spectroscopy-detectable mobile macromolecular proton concentration was higher in human brain tumors than in normal white matter, and increased with tumor grade. APT MRI expands the range of molecular MRI techniques by allowing indirect detection of the amide proton signals in the backbone of endogenous proteins and peptides. According to current theory (Supplementary Methods), the APT imaging signal in tissue is primarily related to two factors: the mobile amide proton content and the amide proton exchange rate, a parameter that depends on tissue pH. Fortunately, despite a low extracellular pH, only a small intracellular pH change (actually, an increase < 0.1 unit) is often detected in tumor tissue[31],[32], allowing the increased APT intensities in tumors to be attributed mainly to increased cytosolic protein and peptide content.

Radiation-induced injury can have many manifestations, both clinically and pathologically[33]. There are three widely recognized syndromes: acute radiation toxicity (occurring during or immediately after radiation); subacute toxicity (occurring up to six months after radiation); and late toxicity (six months to several years after radiation). All of these pathologies show a signal abnormality on T_2-weighted or FLAIR images, and new or increasing amounts of Gd enhancement in the area of radiation, which are indistinguishable from tumor recurrence. The low APT MRI signals in the necrotic lesions are likely associated with the absence of mobile cytosolic proteins and peptides due to the loss of the cytoplasm. Tumors, conversely, are highly cellular, showing hyperintensities on APT images. Thus, the APT signals are an excellent imaging biomarker for the presence of the tumor, while not being very sensitive to radiation necrosis. Our results in this study clearly

demonstrate that APT MRI can provide important complementary information that will greatly improve the value of MRI in the differential diagnosis between viable tumors and radiation injury in patients (Supplementary Discussion).

METHODS

Methods and any associated references are available in the online version of the paper at http://www.nature.com/naturemedicine/.

ONLINE METHODS

Radiation necrosis model

All experiments were approved by the Johns Hopkins Animal Care and Use Committee. We irradiated ten healthy Fischer 344 rats (male; 8–10 weeks; 200–250 g) and five U87MG glioma-bearing nude rats (Supplementary Methods) with the small animal radiation research platform[25]. These animals were anesthetized (4% isoflurane in oxygen in a box for about 5 min for induction, followed by breathing of 2–2.5% isoflurane through a nose cone during radiation) and continuously immobilized in a custom-made plastic cranial fixation device that supported gas anesthesia. A single, well-collimated x-ray beam (single dose, 40 Gy; area, 10 × 10 mm^2) was delivered to the left hippocampus region or to the tumor region under image guidance with planar radiographs, and the other brain regions received a negligible dose. The animals were released into their cages and received lab chow and water ad lib. We monitored the animals with anatomical MR imaging (T_2- and T_1-weighted) monthly until they were sacrificed.

MRI experiments

We acquired MRI data using a horizontal bore 4.7 T Biospec animal imager (Bruker Biospin) with an actively decoupled cross-coil setup (a 70-mm body coil for radiofrequency transmission and a 25-mm surface coil for signal reception). Local shimming was performed on the brain.

First, high-resolution T_2-weighted imaging with fast spin echo acquisition (echo train length = 8; repetition time = 3 s; echo time = 64 ms; 5 slices; slice thickness 1.5 mm; number of averages = 2) was acquired in both the horizontal plane (matrix = 256 × 192; field of view = 42 × 32 mm^2) and the coronal plane (matrix = 192 × 192; field of view = 32 × 32 mm^2). Then, APT images were acquired using frequency-labeling offsets of ±3.5 ppm with respect to water (repetition time = 10 s; echo time = 30 ms; saturation power = 1.3 μT; saturation time = 4 s; 16 averages). A control image in the absence of radiofrequency saturation was also acquired for imaging signal intensity normalization. Single-shot, spin-echo, echo-planar imaging was used for data acquisition (matrix = 64 × 64; field of view = 32 × 32 mm^2; single-slice; slice thickness = 1.5 mm). The image slice was overlapped with one of the T_2-weighted images. Finally, T_1-weighted images (repetition time = 700 ms; echo time = 10 ms; number of average = 10) with and without Gd enhancement were acquired with the same geometry and location as the T_2-weighted images.

APT data analysis

All data processing procedures were performed by Interactive Data Language (IDL; Research Systems, Inc.). The APT images were calculated based on our previously developed theory (Supplementary Methods), and the obtained images were interpolated to 384 × 384, thresholded based on the S_0 image and displayed using a window of −10% to 10%. After shimming and adjustment of the scanner transmitter frequency (Supplementary Methods), no further B_0 inhomogeneity correction was performed for the APT data processing in this study. For the quantitative analysis of APT imaging, we used the signal abnormalities on the high-resolution T_2-weighted images or Gd-enhanced T_1-weighted images as a basis for defining regions of interest. For all rats, these regions of interest (tumor or radiation necrosis) covered most areas of the lesions with the signal abnormalities on MRI (Supplementary Fig. 2). We used contralateral normal-appearing, relatively homogenous brain tissue for comparison. Ventricles and peritumoral edema were excluded.

Statistical analysis

The average APT imaging intensities for the tumors, radiation necrosis, and the corresponding contralateral brain tissue were calculated for each group, and the results were represented as mean ± standard deviation. We calculated the APT MRI contrasts between the tumors and the contralateral brain tissue, as well as between the radiation necrosis and the contralateral brain tissue. A paired t-test was used to determine whether these contrasts were significant. Moreover, we evaluated the differences in APT intensity values between the tumors and radiation necrosis. An unpaired t-test was used to determine whether the observations were significant. We used the analysis of variance (ANOVA) post-hoc tests to determine whether the differences in APT intensities for viable and irradiated glioma were significant. 95% confidence intervals were calculated for the mean contrasts. The level of significance was set at $P < 0.05$.

Additional methods

Detailed methodology is described in the Supplementary Methods.

Supplementary Material

Refer to Web version on PubMed Central for supplementary material.

ACKNOWLEDGMENTS

This work was supported by the US National Institutes of Health grants EB009112, EB009731 and P41 RR015241, and by the DANA Foundation, American Physicians Fellowship, and Brain Tumor Funders' Collaborative. The authors thank J. Zhang for help in pathology experiments and M. McAllister for editorial assistance. SF188/V+ cells used in this study were a generous gift from Dr. Jim Gallo (Temple University, Philadelphia, PA).

References

1. Wen PY, Kesari S. Malignant gliomas in adults. N. Engl. J. Med. 2008; 359:492–507. [PubMed: 18669428]
2. Waldman AD, et al. Quantitative imaging biomarkers in neuro-oncology. Nat. Rev. Clin. Oncol. 2009; 6:445–454. [PubMed: 19546864]

3. Burger PC, et al. Computerized tomographic and pathologic studies of the untreated, quiescent, and recurrent glioblastoma multiforme. J. Neurosurg. 1983; 58:159–169. [PubMed: 6294260]
4. Kumar AJ, et al. Malignant gliomas: MR imaging spectrum of radiation therapy- and chemotherapy-induced necrosis of the brain after treatment. Radiology. 2000; 217:377–384. [PubMed: 11058631]
5. Mullins ME, et al. Radiation necrosis versus glioma recurrence: conventional MR imaging clues to diagnosis. AJNR Am. J. Neuroradiol. 2005; 26:1967–1972. [PubMed: 16155144]
6. Sugahara T, et al. Posttherapeutic intraaxial brain tumor: The value of perfusion-sensitive contrast-enhanced MR imaging for differentiating tumor recurrence from nonneoplastic contrast-enhancing tissue. AJNR Am. J. Neuroradiol. 2000; 21:901–909. [PubMed: 10815666]
7. Chenevert TL, et al. Diffusion magnetic resonance imaging: an early surrogate marker of therapeutic efficacy in brain tumors. J. Nat. Cancer Inst. 2000; 92:2029–2035. [PubMed: 11121466]
8. Smith JS, et al. Serial diffusion-weighted magnetic resonance imaging in cases of glioma: distinguishing tumor recurrence from postresection injury. J. Neurosurg. 2005; 103:428–438. [PubMed: 16235673]
9. Rock JP, et al. Correlations between magnetic resonance spectroscopy and image-guided histopathology, with special attention to radiation necrosis. Neurosurg. 2002; 51:912–919.
10. Chen W. Clinical applications of PET in brain tumors. J. Nucl. Med. 2007; 48:1468–1481. [PubMed: 17704239]
11. Terakawa Y, et al. Diagnostic accuracy of 11C-methionine PET for differentiation of recurrent brain tumors from radiation necrosis after radiotherapy. J. Nucl. Med. 2008; 49:694–699. [PubMed: 18413375]
12. Brandsma D, Stalpers L, Taal W, Sminia P, van den Bent MJ. Clinical features, mechanisms, and management of pseudoprogression in malignant gliomas. Lancet Oncol. 2008; 9:453–461. [PubMed: 18452856]
13. Brandes AA, et al. Disease progression or pseudoprogression after concomitant radiochemotherapy treatment: Pitfalls in neurooncology. Neuro-Oncology. 2008; 10:361–367. [PubMed: 18401015]
14. Yang I, Aghi MK. New advances that enable identification of glioblastoma recurrence. Nat. Rev. Clin. Oncol. 2009; 6:648–657. [PubMed: 19806145]
15. Clarke JL, Chang S. Pseudoprogression and pseudoresponse: Challenges in brain tumor imaging. Curr. Neur. Neurosci. Rep. 2009; 9:241–246.
16. Ward KM, Aletras AH, Balaban RS. A new class of contrast agents for MRI based on proton chemical exchange dependent saturation transfer (CEST). J. Magn. Reson. 2000; 143:79–87. [PubMed: 10698648]
17. Zhou J, van Zijl PC. Chemical exchange saturation transfer imaging and spectroscopy. Progr. NMR Spectr. 2006; 48:109–136.
18. Aime S, et al. High sensitivity lanthanide(III) based probes for MR-medical imaging. Coord. Chem. Rev. 2006; 250:1562–1579.
19. Sherry AD, Woods M. Chemical exchange saturation transfer contrast agents for magnetic resonance imaging. Annu. Rev. Biomed. Eng. 2008; 10:391–411. [PubMed: 18647117]
20. Zhou J, Payen J, Wilson DA, Traystman RJ, van Zijl PCM. Using the amide proton signals of intracellular proteins and peptides to detect pH effects in MRI. Nature Med. 2003; 9:1085–1090. [PubMed: 12872167]
21. Zhou J, Lal B, Wilson DA, Laterra J, van Zijl PCM. Amide proton transfer (APT) contrast for imaging of brain tumors. Magn. Reson. Med. 2003; 50:1120–1126. [PubMed: 14648559]
22. Hobbs SK, et al. Magnetic resonance imaging-guided proteomics of human glioblastoma multiforme. J. Magn. Reson. Imag. 2003; 18:530–536.
23. Howe FA, et al. Metabolic profiles of human brain tumors using quantitative in vivo ^{1}H magnetic resonance spectroscopy. Magn. Reson. Med. 2003; 49:223–232. [PubMed: 12541241]
24. Zhou J, et al. Practical data acquisition method for human brain tumor amide proton transfer (APT) imaging. Magn. Reson. Med. 2008; 60:842–849. [PubMed: 18816868]
25. Wong J, et al. High-resolution, small animal radiation research platform with X-ray tomographic guidance capabilities. Int J Rad Oncol Bio Phys. 2008; 71:1591–1599.

26. Ma J, Zhou-Li F, Klein-Szanto A, Gallo JM. Modulation of angiogenesis by human glioma xenograft models that differentially express vascular endothelial growth factor. Clin. Exp. Metastasis. 1998; 16:559–568. [PubMed: 9872603]
27. Ozawa T, et al. Response of intracerebral human glioblastoma xenografts to multifraction radiation exposures. Int. J. Rad. Onc. Biol. Phys. 2006; 66:263–270.
28. Ross BD, Chenevert TL, Rehemtulla A. Magnetic resonance imaging in cancer research. Eur. J. Cancer. 2002; 38:2147–2156. [PubMed: 12387840]
29. Chenevert TL, Ross BD. Diffusion imaging for therapy response assessment of brain tumor. Neuroimag. Clin. N. Am. 2009; 19:559–571.
30. Padhani AR, et al. Diffusion-weighted magnetic resonance imaging as a cancer biomarker: Consensus and recommendations. Neoplasia. 2009; 11:102–125. [PubMed: 19186405]
31. Griffiths JR. Are cancer cells acidic? Br. J. Cancer. 1991; 64:425–427. [PubMed: 1911181]
32. Gillies RJ, Raghunand N, Garcia-Martin M, Gatenby RA. pH imaging. IEEE Eng. Med. Biol. 2004; 23:57–64.
33. Valk PE, Dillon WP. Radiation injury of the brain. AJNR Am. J. Neuroradiol. 1991; 12:45–62. [PubMed: 7502957]

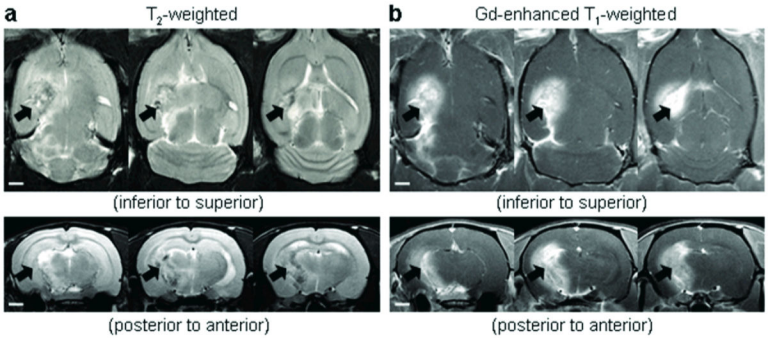

Figure 1.

MRI characteristics of radiation necrosis (40 Gy, 178 days post-radiation; black solid arrow) in a rat. (a) T_2-weighted images. (b) Gd-enhanced T_1-weighted images. Both axial (top row) and coronal (bottom row) planes were acquired, and three consecutive slices are shown. Radiation necrosis is heterogeneous on the T_2-weighted images and shows large enhancement on the Gd-enhanced T_1-weighted images. Scale bars: 2 mm.

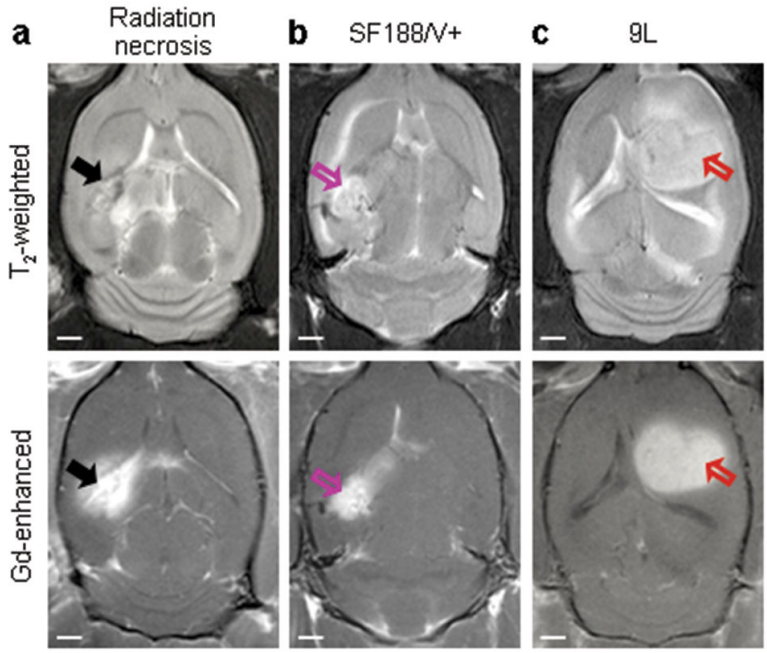

Figure 2.

Comparison of radiation necrosis and glioma by conventional MRI sequences. (a) Radiation necrosis (40 Gy, 178 days post-radiation; black solid arrow). (b) SF188/V+ human glioma (16 days post-implantation; pink open arrow). (c) 9L gliosarcoma (12 days post-implantation; red open arrow). All pathologies are heterogeneous on the T_2-weighted images and show large enhancement on the Gd-enhanced T_1-weighted images. The shifted midlines of the brain indicate possible mass effect. These MRI features are very similar and not predictive of the final pathology. Scale bars: 2 mm.

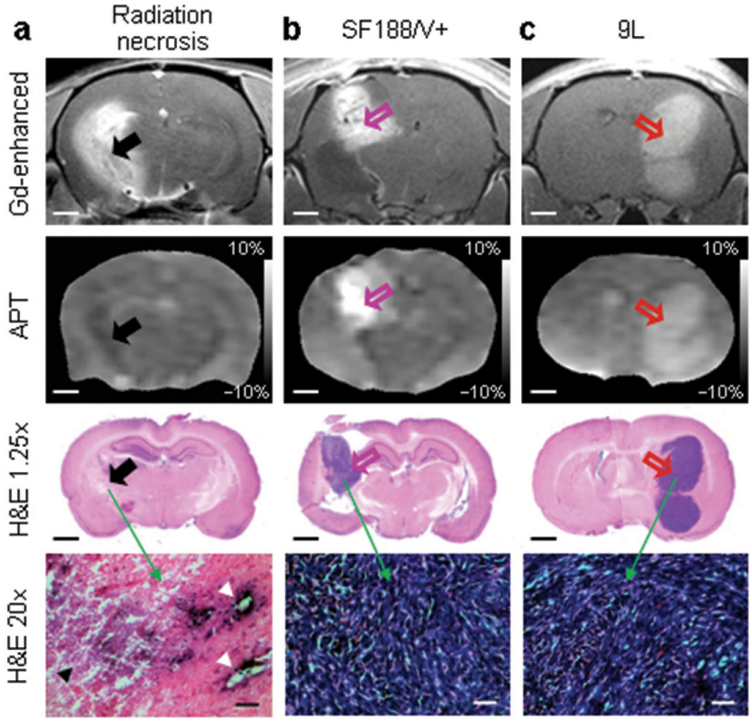

Figure 3.

Comparison of radiation necrosis and glioma using APT MRI and histology. (a) MR images and H&E-stained histopathological sections of radiation necrosis (40 Gy, 178 days post-radiation). Radiation necrosis (black solid arrow) is revealed by Gd enhancement. Compared with contralateral brain tissue, APT MRI is hypointense to isointense in the lesion, where the loss of normal brain tissue components with vacuolation changes of necrosis (black arrowhead), as well as dilated damaged vessels (white arrowhead), are clearly visible on the high-magnification histology images. (b) MR images and H&E staining of SF188/V+ human glioma (16 days post-implantation). (c) MR images and H&E staining of 9L gliosarcoma (11 days post-implantation). Both SF188/V+ (pink open arrow) and 9L (red open arrow) tumors are hyperintense on the APT images, corresponding to high cellularity on histology. Scale bars: 2 mm (Gd-enhanced, APT and H&E 1.25×) and 50 μm (H&E 20×).

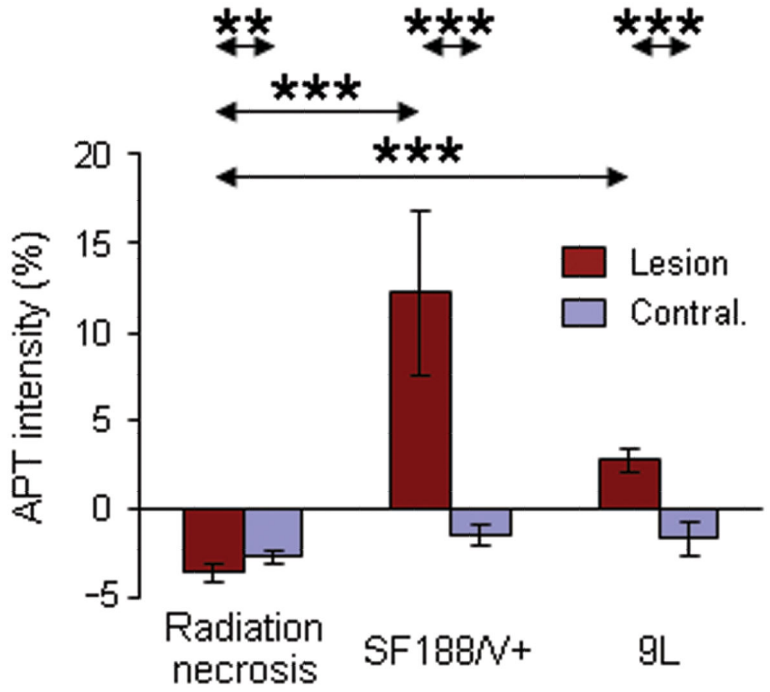

Figure 4.

Quantitative comparison of APT image intensities (in % change of the bulk water signal intensity) for radiation necrosis and glioma. Radiation necrosis (40 Gy, 163–188 days post-radiation, $n = 9$); SF188/V+ human glioma (9–35 days post-implantation, $n = 9$); 9L gliosarcoma (10–12 days post-implantation, $n = 9$). ** $P < 0.05$; *** $P < 0.001$. The tumors and radiation necrosis have opposite APT signal intensities with respect to the contralateral brain tissue.

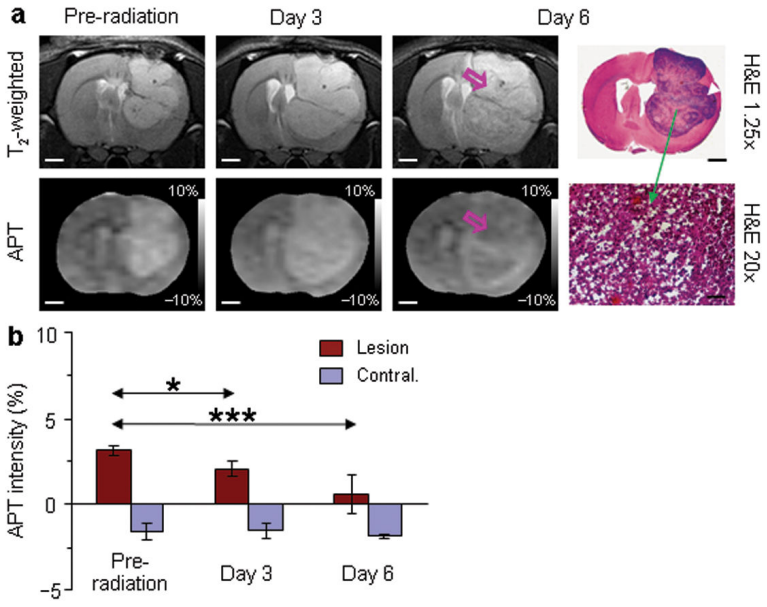

Figure 5.

Changes in APT signal intensity (in % change of the bulk water signal intensity) for the radiated U87MG tumors as a function of time post-radiation (40 Gy; pre-radiation, 3 days and 6 days post-radiation). (a) T_2-weighted and APT images and H&E-stained brain sections for a typical rat. Prior to radiation, tumors are hyperintense with minimal heterogeneity on the APT images. APT signals show a clear decrease following therapy. At 6 days post-radiation, the image intensity of the mass is very heterogeneous with an area that is almost isointense to contralateral normal tissue (pink arrow). At this time point, the presence of severe radiation necrosis was confirmed on histology. Low density tumor cells were also found mainly on the edge of the lesion (white arrowhead). Scale bars: 2 mm (T_2-weighted, APT and H&E 1.25×) and 50 μm (H&E 20×). (b) Quantitative comparisons of APT image intensities for the irradiated tumors and the contralateral normal-appearing brain tissue. n = 5; * $P < 0.05$; *** $P < 0.001$. The average APT signal intensities in the lesion significantly decrease at 3 days and 6 days post-radiation ($P < 0.05$ and $P < 0.001$, respectively).